PAPER

Check for updates

Hierarchical branched α-MnO$_2$: one-step synthesis and catalytic activity†

Hengfa Liu, Bentian Zhang, Wanping Li, Gao Cheng, Jiaxi Han, Bang Lan, Ming Sun [iD] * and Lin Yu [iD]

Hierarchical pine tree-like α-MnO$_2$ architectures are prepared by a facile one-step method without any template. The hierarchical α-MnO$_2$ is composed of branched α-MnO$_2$ short nanorods assembled onto the backbone of an α-MnO$_2$ long nanowire. Time-dependent experiment shows that the growth process of the branched α-MnO$_2$ nanostructures is the formation of β-MnOOH and then the transformation to a α-MnO$_2$ branched structure in a step by step manner. Owing to its specific structure features, the hierarchical pine tree-like α-MnO$_2$ exhibits superior catalytic performance in the catalytic combustion of dimethyl ether with a light-off temperature (T_{10}) at 169 °C and a complete conversion temperature (T_{90}) of 235 °C, which is far better than commercial MnO$_2$.

1   Introduction

The rational design and preparation of hierarchical structures has great significance because of their morphology and size dependent properties. The hierarchical architectures possess multifunctional and collective properties, and have found wide applications in heterogeneous catalysis, photo-catalysis and electrochemistry.[1] Therefore, much efforts have been focused on this special functional material.

As a transition metal oxide with rich sources and wide usages, the MnO$_2$ material has attracted great interest due to its excellent physical and chemical properties.[2–4] And such properties are highly dependent on the morphology and crystalline structure of MnO$_2$. To date, many efforts have been made to synthesize MnO$_2$ with different morphology and crystal phase aiming to explore better activities. Also, there are some reports on the hierarchical MnO$_2$ based architectures. Careful study the reported papers we can find that: (1) the preparation of hierarchical MnO$_2$ usually involves multistep process,[5–7] or using template assistance,[8–11] or with metal ions assistance;[12–14] (2) the morphology of the obtained MnO$_2$ materials is mainly confined to microsphere *via* hydrothermal process which is energy consuming, for example, α-MnO$_2$,[15–17] γ-MnO$_2$,[12,14,18,19] δ-MnO$_2$,[20,21] OMS-1,[22] ε-MnO$_2$.[23] The hierarchical MnO$_2$ with other shape instead of sphere is rare except the star-like[24] and the branched α-MnO$_2$,[11,25,26] the β-MnO$_2$ nanopincer,[27] star-like ε-MnO$_2$,[28] and the δ-MnO$_2$ hollow nanobox;[29] Therefore, it is still

a challenge to develop an easy and temple-free method to prepare hierarchical MnO$_2$ with new morphology other than the commonly obtained sphere-like shape. The complexity and creativity in structure may bring new properties to the MnO$_2$ functional materials,[18] and further favoring for their potential application.

Herein, we present a facile method to prepare the α-MnO$_2$ hierarchical architecture with pine tree-like morphology. The formation is accomplished by one-step reaction between MnCO$_3$ and (NH$_4$)$_2$S$_2$O$_8$ in H$_2$SO$_4$ solution at room temperature. The strategy has the merit of one-step synthesis at room temperature without any template or chelating ligand. As a typical example, the prepared pine tree-like α-MnO$_2$ has been evaluated as catalyst for the catalytic combustion of dimethyl ether (DME), and exhibited better performance than that of the commercial MnO$_2$.

2   Experimental

The MnCO$_3$ were obtained from Aladdin, the (NH$_4$)$_2$S$_2$O$_8$ and condensed H$_2$SO$_4$ (98 wt%) were bought from Guangzhou Chemical Agent Factory. They were used as received. In a typical synthesis, 20 mmol (NH$_4$)$_2$S$_2$O$_8$ and 20 mL H$_2$SO$_4$ were dissolved in 400 mL distilled water to form the transparent solution in a beaker, then 20 mmol MnCO$_3$ was introduced. The solution was magnetically stirring at room temperature for 54 h. Afterward, the products were filtered and washed with ethanol solution and dried at 60 °C for further use.

A Brucker D8-advance X-ray diffractometer was used to test the crystal structure of the products, operating at 40 kV, and 40 mA at a scan rate of 4° min^{-1}. The morphology of the MnO$_2$ were studied on a scanning electron microscopy (SEM, HITA-CHI SU8010) and a transmission electron microscopy (TEM,

---

Key Laboratory of Clean Chemistry Technology of Guangdong Regular Higher Education Institutions, School of Chemical Engineering and Light Industry, Guangdong University of Technology, Guangzhou, 510006, P. R. China. E-mail: sunmgz@gdut.edu.cn; Fax: +86-20-39322231; Tel: +86-20-39322202

FEI, Tecnai G2 F20). The Mn 2p, O 1s spectra were obtained on the X-ray photoelectron spectroscopy (XPS, Thermo ESCALAB 250) equipped with a monochromatic Al Kα (1486.6 eV) X-ray source. The temperature programmed reduction of hydrogen (H_2-TPR) of MnO_2 was tested on Autochem 2920 (Micromeritics) instrument, 30 mg of sample was used and pretreated at 200 °C in a flow of Ar for 1 h. Afterwards, the catalyst was heated from 50 °C to 600 °C at a rate of 10 °C min^{-1} in a flowing 5 vol% H_2/Ar mixture (50 mL min^{-1}).

The catalytic combustion of dimethyl ether was performed in a continuous flow fixed-bed reactor (8 mm i.d.). The loading amount of MnO_2 was 100 mg with 100 mg of quartz sands. A gas mixture of DME, oxygen and helium were co-feed into the reactor with the volume ratio of 1 : 10 : 40, and the total gas hourly space velocity was 30 000 h^{-1}. The out-flow gas was analyzed by gas chromatograph (Agilent 6820).

3   Results and discussion

The pine tree-like manganese oxide was synthesized by a one-step solution route. The crystal structure of the as-prepared products (54 h) was investigated by X-ray powder diffraction (XRD). As shown in Fig. 1a, all the peaks can be indexed to pure α-MnO_2 (JCPDS 44-0141) without any impurity. The product was further characterized by XPS to test the element composition and chemical state. The survey and Mn 2p spectra are displayed in Fig. 1c and b, respectively. The survey spectrum shows characteristic peaks for Mn, O and C, which is similar to that

reported.[30] In Fig. 1b, we can see clearly two major XPS peaks of Mn 2p$_{3/2}$ at 642.2 eV and Mn 2p$_{1/2}$ at 654.0 eV, which confirmed the presence of MnO_2.[31,32]

The morphology of the final product was studied by SEM and TEM as displayed in Fig. 2. The SEM images in Fig. 2a show that the α-MnO_2 displays perfect pine tree-like nanostructures with high dispersity. On closer inspection (Fig. 2b and c), the hierarchical branched α-MnO_2 structure is composed by a long nanowire as backbone with homogenously covered short nanorods having a uniform length of *ca.* 322 nm (ESI, Fig. S1,† based on 50 branched pedals selected randomly in 5 SEM images). The length of pine tree-like nanostructures extends to several micrometers, resulting in exceptionally large aspect ratio. The detailed structure of the branched α-MnO_2 was further investigated using TEM (Fig. 2d) and HRTEM (Fig. 2e and f). As displayed in Fig. 2d, the core nanowire is wrapped by numerous nanorods interconnected with each other. The diameter of the core nanowire is about 200 nm. The HRTEM of the branch nanorod (Fig. 2f) demonstrates a interplanar spacing of 0.24 nm, corresponding to the (211) planes of α-MnO_2. The HRTEM image of the interface of the core and the branch is shown in Fig. 2e. Across the interface, we can detect that two kind of lattices fringes of 0.31 nm and 0.24 nm, which belong to the (310) plane of α-MnO_2 core nanowire and the (211) planes of α-MnO_2 branch nanorod, respectively.[33,34]

The N_2 adsorption–desorption isotherms (Fig. 3) of the sample can be assigned to the isothermals of type II according to the IUPAC classification, indicating that the pine tree-like α-
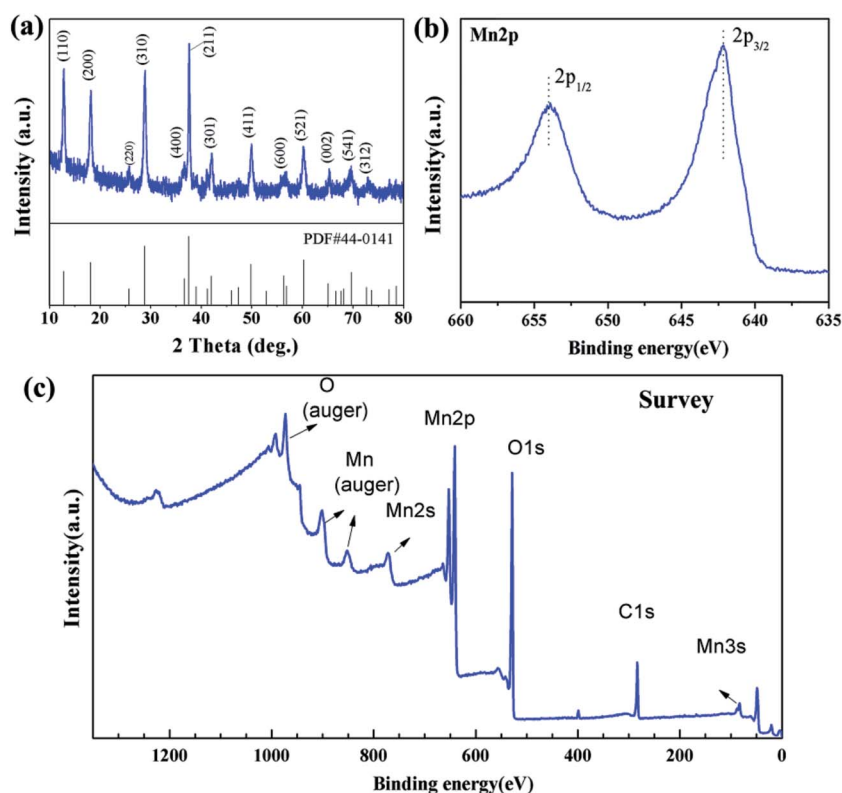

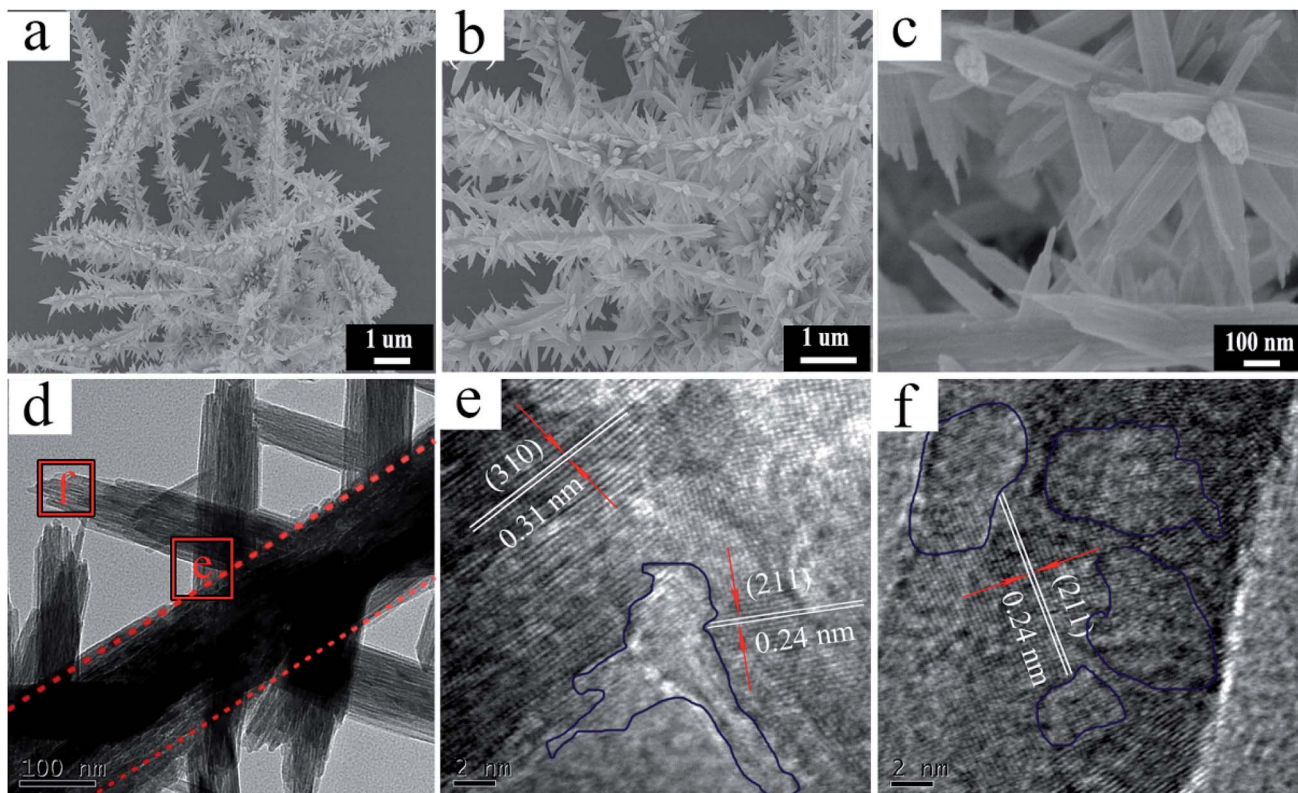**Fig. 1** XRD pattern (a) and XPS spectra (b, Mn 2p; c, survey) of the hierarchical branched α-MnO_2.

Fig. 2 SEM (a–c), TEM (d) and HRTEM (e–f) images of the hierarchical branched α-MnO$_2$.
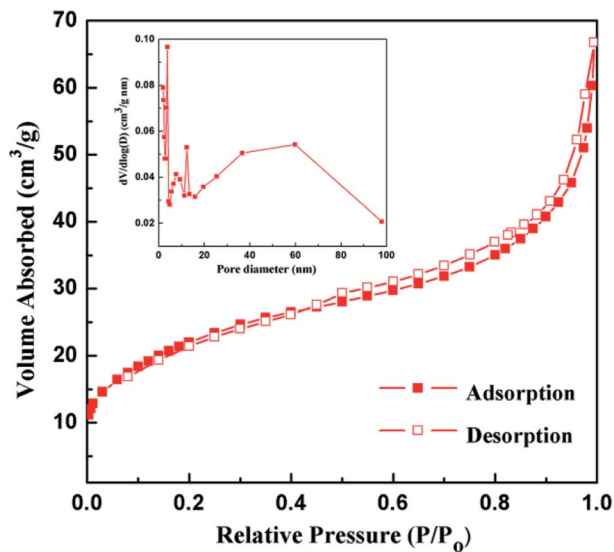

Fig. 3 The N$_2$ adsorption–desorption isotherms and pore size distribution of the hierarchical branched α-MnO$_2$.

MnO$_2$ nanostructures belong to typical mesoporous material. The measured BET surface area of the α-MnO$_2$ is 77.5 m^2 g^{-1}. Based on the pore size distribution, we can find that the hierarchical branched α-MnO$_2$ has rich pore structures, locating at around three narrow ranges of 3.7, 7.6, and 12.4 nm, and a wide range from 15 to 100 nm.

To explore the formation process of the pine tree-like nanostructure, time-dependent experiment was carried out and the corresponding SEM images are exhibited in Fig. 4. At the first hour, we can see that nanorod or wire-like MnOOH is formed, however, the chemical source MnCO$_3$ still remains in the reaction system as marked by the red arrow in Fig. 4a (the morphology of the MnCO$_3$ is provide in the ESI, Fig. S2,† showing plate packed structure). When the reaction time is 4 h, the obtained product demonstrates the typical shape of nanowires of several micrometers with smooth surface (Fig. 4b). As the time increased to 15 h, very tiny nanorods are formed over the surfaces of the nanowires (Fig. 4c). The tiny nanorods are continuously to grow richer and bigger with reaction time rising to 26 h (Fig. 4d). From the inset figure in Fig. 4d, the smooth surface of the nanowire becomes rough, and even with small hole formed. When the reaction time is 37 h, the short nanorods are continuously deposited over the β-MnOOH nanowires surface forming branched structure (Fig. 4e). The inset figure in Fig. 4e demonstrates that the branched petals are becoming condensed. Further elongating the reaction time to 48 h, the hierarchical branched product turns to more complex and the size become even bigger (Fig. 4f). The pine tree-like morphology began to form. Finally, the pure phase of α-MnO$_2$ with fine hierarchical architecture is obtained when the reaction time is 56 h (Fig. 2).

The crystal structures of the intermediate product at certain stage are studied by XRD, and the results are exhibited in Fig. 5. At a time of 4 h, the nanowire product shows a pure β-MnOOH
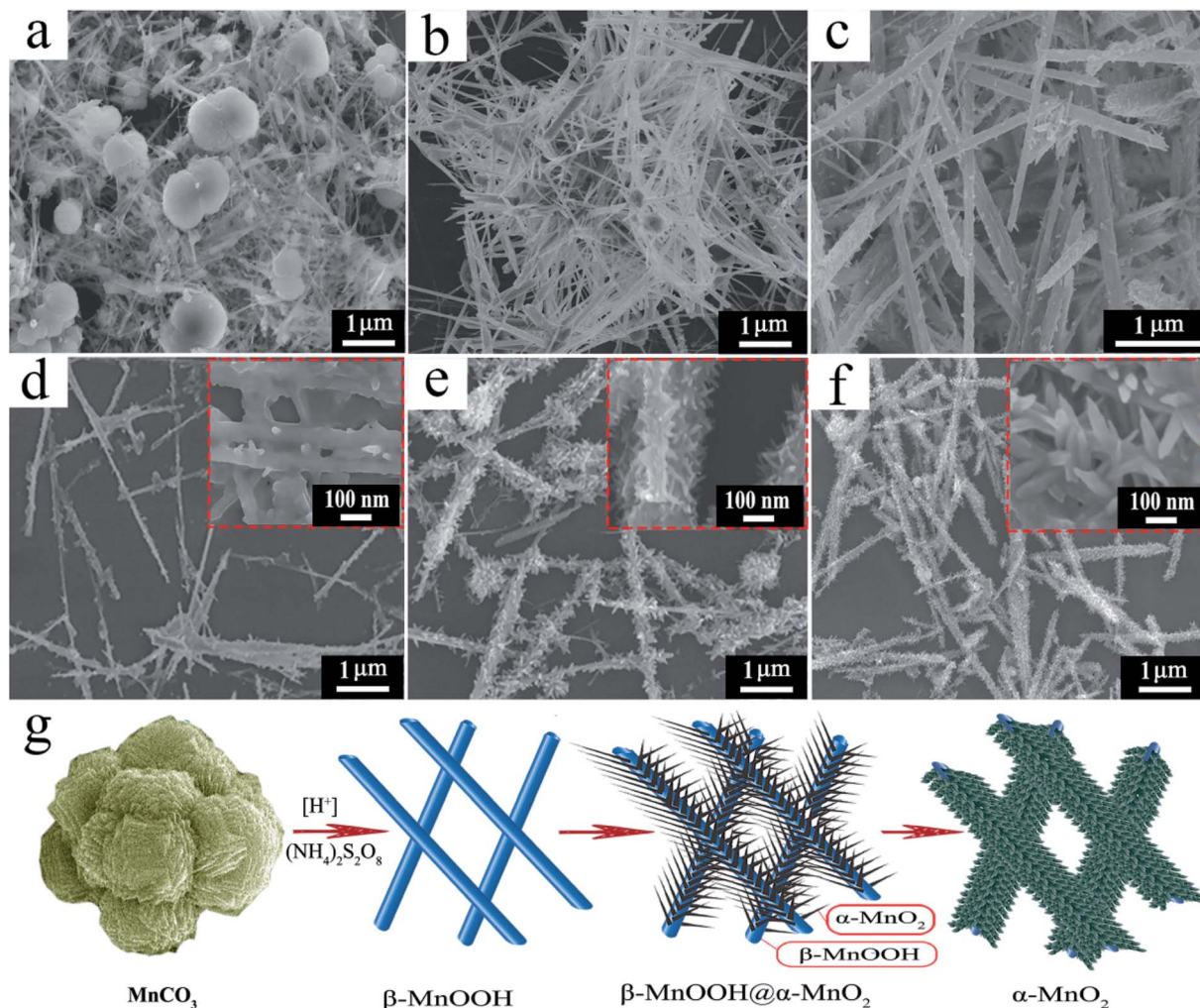
Fig. 4 SEM images of the sample at different stage: (a) 1 h, (b) 4 h, (c) 15 h, (d) 26 h, (e) 37 h (f) 48 h; and (g) schematic illustration of the synthetic process of the α-MnO₂.
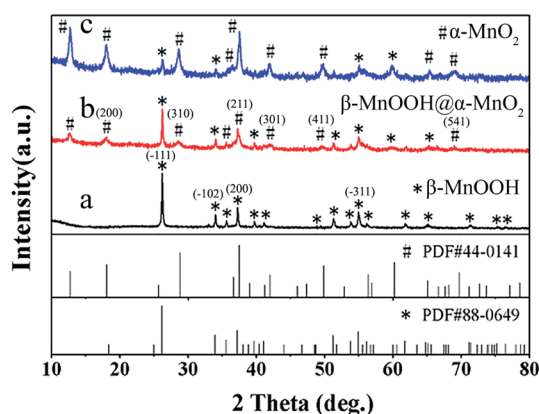

Fig. 5 XRD patterns of the sample under (a) 4 h, (b) 26 h, (c) 48 h.

phase (JCPDS 88-0649) as depicted in Fig. 5a. The sharp and intense diffraction peaks indicate that the product has good crystallinity. As the time rise to 26 h (Fig. 5b), the intensity of the β-MnOOH peaks become weaken, while new peaks of (200),
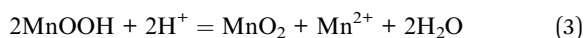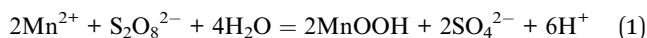
(310), (211), (301), (411) and (541) are forming, and they are belonging to the α-MnO₂ (JCPDS 44-0141). According to the corresponding SEM image in Fig. 4d, the tiny nanorod around the surface of the MnOOH has a crystal structure of α-MnO₂. When the reaction time rises to 48 h, the dominate structure evolves into α-MnO₂ with minority phase of β-MnOOH nanowire as proved by the XRD analysis (Fig. 5c). Finally, at 56 h, pure phase of α-MnO₂ are synthesized without any impurity (Fig. 1a).

In the formation of the pine tree-like hierarchical branched α-MnO₂, the role of MnCO₃ is vital important. When we change MnCO₃ into other source of Mn²⁺, we can not obtain the pine-tree like α-MnO₂. Fig. S3† lists the SEM images by using $Mn(NO_3)_2$ and $MnSO_4$ instead of MnCO₃ at the same reaction conditions. We can clearly see that they show the shape of 3D urchin sphere composed by short nanorod, which is commonly observed in the reported literatures.[17–19,35]

In our reaction system, the MnCO₃ is in solid state, and this is different from other commonly used Mn²⁺ source, which can be dissolved in the solvent. With condensed H_2SO_4 present in

the reaction system, the $MnCO_3$ will erode by the acid gradually and produce soluble $MnSO_4$ (many bubbles of CO_2 are observed at the first stage of the reaction; under the reaction conditions, the $MnCO_3$ could be observed in the beginning 1 h). At the same time, the newly formed $MnSO_4$ would react with $S_2O_8^{2-}$ to obtain $MnOOH$ firstly (eqn (1)), as proved by the SEM image is Fig. 4a. This is because that the dissolve of $MnCO_3$ consuming large amount of acid, and less acid reduce the oxidation ability of the reaction system, the $MnOOH$ will form preferentially.[32] The formation of $MnOOH$ is very quick (less in a hour) with extra H^+ forming. Having enough H^+ in the reaction system, the Mn^{2+} can be further oxided to MnO_2 under the assistance of NH_4^+. Then two parallel reaction might happen: (a) the $MnOOH$ could transform to MnO_2 under the work of acid through a dissolution–recrystallization process (eqn (3)).[32,36,37] The dissolution of $MnOOH$ is clearly demonstrated by the SEM image in Fig. 4d; (b) the remaining Mn^{2+} could react with $S_2O_8^{2-}$ producing MnO_2 (eqn (2)). To reduce the system energy, the newly formed MnO_2 nano-crystal prefer to grow over the surface of $MnOOH$, and to use $MnOOH$ as the seed to grow via oriented attachment.

$$2Mn^{2+} + S_2O_8^{2-} + 4H_2O = 2MnOOH + 2SO_4^{2-} + 6H^+ \quad (1)$$

$$Mn^{2+} + S_2O_8^{2-} + 2H_2O = MnO_2 + 2SO_4^{2-} + 4H^+ \quad (2)$$

$$2MnOOH + 2H^+ = MnO_2 + Mn^{2+} + 2H_2O \quad (3)$$

The branched α-MnO_2 was examined as a catalyst for the catalytic combustion of DME. The commercial MnO_2 was also evaluated for comparison, and the result is shown in Fig. 6a. Apparently, the branched α-MnO_2 outperformed commercial MnO_2, with a light-off temperature (T_{10}) at 169 °C and a complete conversion temperature (T_{90}) at 235 °C. For the commercial MnO_2, the T_{10} is 282 °C and T_{90} is more than 430 °C. Considering the complete conversion temperature, the branched α-MnO_2 has the higher catalytic activity than the commercial MnO_2. The apparent activation energy (E_a) of the DME combustion over the two MnO_2 catalysts was calculated. From Fig. 6b, the E_a for commercial MnO_2 and hierarchical α-MnO_2 is 87.24 and 64.98 KJ mol^{-1}, meaning that the catalytic combustion of DME could operate more easily over the branched α-MnO_2 than commercial one.

To explain the difference in their catalytic performance, H_2-TPR and XPS experiments were carried on. The reduction profile of the commercial MnO_2 is similar to many of the reported MnO_2, of which only one wide peak is observed.[17,38] The overlapped peak of the commercial MnO_2 is centered at 515 °C, which contains the reduction process from Mn^{4+} to Mn^{3+} then to Mn^{2+} (Fig. 6c). Whereas, the TPR profile of the hierarchical α-MnO_2 is different from the commercial and the conventional α-MnO_2. We can detect one sharp peak at 265 °C and another continuous peak. This is a reflection of both the reduction of Mn^{4+} to Mn^{2+} and reduction from the branched part to the backbone part of MnO_2. Careful comparison of the temperature of the reduction peak, the reducibility of the two MnO_2 dropped in the order of pine tree-like α-MnO_2 > commercial MnO_2, and this agrees well with their catalytic performance. The mobility of oxygen species has great effect on the combustion activity. The higher reducibility indicates that the branched α-MnO_2 has higher mobility of the oxygen species, which would lead to a better catalytic activity.[39,40] XPS measurement was used to study the oxygen species. The O 1s spectral result of the
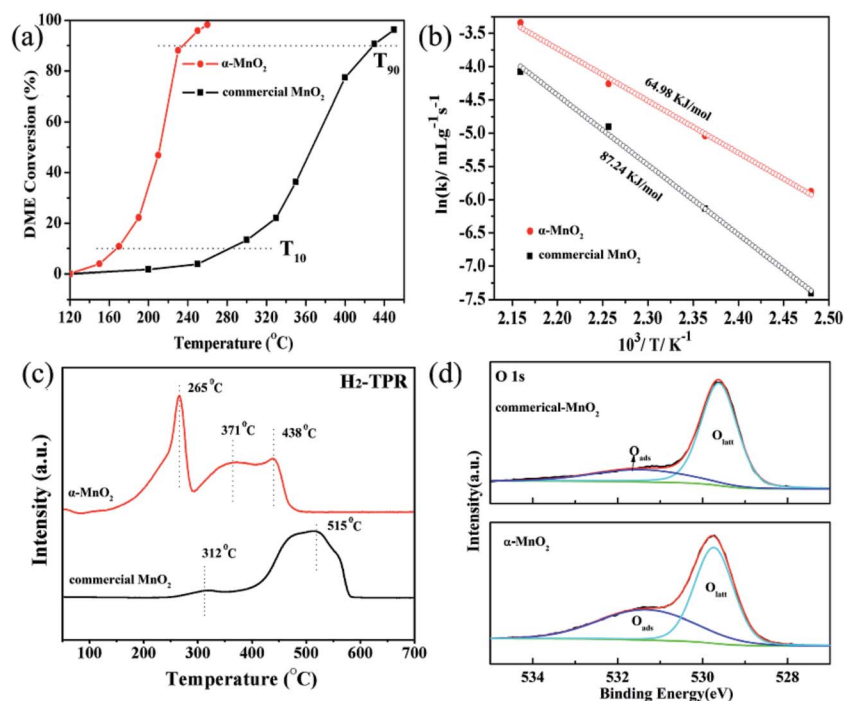

Fig. 6 DEM combustion performance (a), Arrhenius plots (b), H_2-TPR profiles (c) and O 1s XPS spectra (d) of the two MnO_2.

branched α-MnO$_2$ is shown in Fig. 6d. The binding energy at 529.7 eV belongs to the lattice oxygen species and the binding energy at 531.3 eV is attributed to the surface defective oxygen.[41] The O$_{ads}$/O$_{latt}$ molar ratios of the branched α-MnO$_2$ is 0.84, which is larger than that of the commercial MnO$_2$(0.27). Therefore, the pine-tree like α-MnO$_2$ has a large amounts of surface oxygen vacancy, and this is helpful for the catalytic performance.[42,43]

4 Conclusions

In summary, we have developed a facile one-step strategy without any template to synthesize the hierarchical pine tree-like α-MnO$_2$ nanostructures, which is easily scaled up for mass production. The source of Mn (MnCO$_3$) is considered to play an important role in the formation of α-MnO$_2$ branched architectures. Our findings not only show that the pine tree-like α-MnO$_2$ has an outstanding catalytic activity for DME combustion, but also provide a method to synthesize novel hierarchical materials, which may possess potential applications in other fields.

Conflicts of interest

There are no conflicts to declare.

Acknowledgements

References

1 M. H. Sun, S. Z. Huang, L. H. Chen, Y. Li, X. Y. Yang, Z. Y. Yuan and B. L. Su, *Chem. Soc. Rev.*, 2016, **45**, 3479–3563.
2 Z. Chen, Z. Jiao, D. Pan, Z. Li, M. Wu, C.-H. Shek, C. M. L. Wu and J. K. L. Lai, *Chem. Rev.*, 2012, **112**, 3833–3855.
3 M. M. Najafpour, M. Hołyńska and S. Salimi, *Coord. Chem. Rev.*, 2015, **285**, 65–75.
4 H. Sun, Y. Shang, K. Xu, Y. Tang, J. Li and Z. Liu, *RSC Adv.*, 2017, **7**, 30283–30288.
5 W. Xiao, P. Zhou, X. H. Mao and D. H. Wang, *J. Mater. Chem. A*, 2015, **3**, 8676–8682.
6 P. Pal, S. K. Pahari, A. K. Giri, S. Pal, H. C. Bajaj and A. B. Panda, *J. Mater. Chem. A*, 2013, **1**, 10251–10258.
7 B. Zhang, G. Cheng, W. Ye, X. Zheng, H. Liu, M. Sun, L. Yu, Y. Zheng and X. Cheng, *Dalton Trans.*, 2016, **45**, 8.
8 D. Sun, J. Chen, J. Yang and X. Yan, *CrystEngComm*, 2014, **16**, 10476–10484.
9 M. Du, Y. Bu, Y. Zhou, Y. Zhao, S. Wang and H. Xu, *RSC Adv.*, 2017, **7**, 12711–12718.
10 J. Ma, Q. Cheng, V. Pavlinek, P. Saha and C. Li, *New J. Chem.*, 2013, **37**, 722–728.

11 B. Z. Yu, X. Dan Zhao, J. Luo, H. G. Zhang, Y. W. Zhu, G. Y. Jing, P. Ma, Z. Y. Ren and H. M. Fan, *Adv. Mater. Interfaces*, 2016, **3**, 1500761.
12 D. Y. Li, X. F. Wu and Y. F. Chen, *J. Phys. Chem. C*, 2013, **117**, 11040–11046.
13 B. Li, G. Rong, Y. Xie, L. Huang and C. Feng, *Inorg. Chem.*, 2006, **45**, 6404–6410.
14 X. Ge, J. Liu, X. Song, G. Wang, H. Zhang, Y. Zhang and H. Zhao, *Chem. Eng. J.*, 2016, **301**, 139–148.
15 P. Yu, X. Zhang, D. Wang, L. Wang and Y. Ma, *Cryst. Growth Des.*, 2008, **9**, 528–533.
16 Z. Li, Y. Ding, Y. Xiong, Q. Yang and Y. Xie, *Chem. Commun.*, 2005, 918–920.
17 T. Lin, L. Yu, M. Sun, G. Cheng, B. Lan and Z. Fu, *Chem. Eng. J.*, 2016, **286**, 114–121.
18 D. Li, J. Yang, W. Tang, X. Wu, L. Wei and Y. Chen, *RSC Adv.*, 2014, **4**, 26796–26803.
19 R. Chen, J. Yu and W. Xiao, *J. Mater. Chem. A*, 2013, **1**, 11682.
20 H. Jiang, T. Sun, C. Li and J. Ma, *J. Mater. Chem.*, 2012, **22**, 2751–2756.
21 S. Bag and C. R. Raj, *J. Mater. Chem. A*, 2016, **4**, 8384–8394.
22 H. J. Cui, J. W. Shi, F. Liu and M. L. Fu, *J. Mater. Chem.*, 2011, **21**, 18527–18529.
23 D. Han, X. Jing, P. Xu, Y. Ding and J. Liu, *J. Solid State Chem.*, 2014, **218**, 178–183.
24 G. Cheng, S. Xie, B. Lan, X. Zheng, F. Ye, M. Sun, X. Lu and L. Yu, *J. Mater. Chem. A*, 2016, **4**, 16462–16468.
25 X. Zhang, B. Li, X. Li, Q. Chu, M. Yang, X. Wang, H. Chen, L. Peng and X. Liu, *J. Mater. Sci.: Mater. Electron.*, 2014, **25**, 906–913.
26 X. Su, X. Yang, L. Yu, G. Cheng, H. Zhang, T. Lin and F.-H. Zhao, *CrystEngComm*, 2015, **17**, 5970–5977.
27 G. Cheng, L. Yu, T. Lin, R. Yang, M. Sun, B. Lan, L. Yang and F. Deng, *J. Solid State Chem.*, 2014, **217**, 57–63.
28 Y. S. Ding, X. F. Shen, S. Gomez, H. Luo, M. Aindow and S. L. Suib, *Adv. Funct. Mater.*, 2006, **16**, 549–555.
29 J. Zhang, Y. Luan, Z. Lyu, L. Wang, L. Xu, K. Yuan, F. Pan, M. Lai, Z. Liu and W. Chen, *Nanoscale*, 2015, **7**, 14881–14888.
30 J. W. Long, J. M. Wallace, G. W. Peterson and K. Huynh, *ACS Appl. Mater. Interfaces*, 2016, **8**, 1184–1193.
31 Y. Li, Y. Li, Y. Wan, S. Zhan, Q. Guan and Y. Tian, *RSC Adv.*, 2016, **6**, 54926–54937.
32 M. Sun, B. Lan, T. Lin, G. Cheng, F. Ye, L. Yu, X. Cheng and X. Zheng, *CrystEngComm*, 2013, **15**, 7010.
33 B. Zhang, G. Cheng, B. Lan, X. Zheng, M. Sun, F. Ye, L. Yu and X. Cheng, *CrystEngComm*, 2016, **18**, 6895–6902.
34 H. Li, W.-l. Wang, F. Pan, X. Xin, Q. Chang and X. Liu, *Mater. Sci. Eng., B*, 2011, **176**, 1054–1057.
35 Y. Wang, M. Liu, K. Li, A. Zhang and X. Guo, *CrystEngComm*, 2015, **17**, 3636–3644.
36 M. Ramstedt and S. Sjöberg, *Aquat. Geochem.*, 2005, **11**, 413–431.
37 D. Portehault, S. Cassaignon, E. Baudrin and J.-P. Jolivet, *Chem. Mater.*, 2007, **19**, 5410–5417.
38 G. Cheng, L. Yu, B. He, M. Sun, B. Zhang, W. Ye and B. Lan, *Appl. Surf. Sci.*, 2017, **409**, 223–231.

39 H. Sun, Z. Liu, S. Chen and X. Quan, *Chem. Eng. J.*, 2015, **270**, 58–65.

40 Q. Ye, H. Lu, J. Zhao, S. Cheng, T. Kang, D. Wang and H. Dai, *Appl. Surf. Sci.*, 2014, **317**, 892–901.

41 V. P. Santos, M. F. R. Pereira, J. J. M. Orfao and J. L. Figueiredo, *Appl. Catal., B*, 2010, **99**, 353–363.

42 S. H. Xie, J. G. Deng, S. M. Zang, H. G. Yang, G. S. Guo, H. Arandiyan and H. X. Dai, *J. Catal.*, 2015, **322**, 38–48.

43 M. Sun, L. Yu, F. Ye, G. Q. Diao, Q. Yu, Z. F. Hao, Y. Y. Zheng and L. X. Yuan, *Chem. Eng. J.*, 2013, **220**, 320–327.